CHAPTER 7

TRANSPORT PROPERTIES OF NBR/EVA BLENDS

The results of this chapter have been communicated to *J. Polym. Sci.-Polym. Phys.*

Transport of organic solvents through polymeric materials have been a subject of fundamental interest[1-5] and the technological importance of the molecular transport of solvents in polymers play a vital role in a variety of applications such as separation process,[6] food packaging,[7] controlled drug release,[8] reverse osmosis[9] and microelectronics.[10] As far as these applications are concerned it is quite essential to evaluate the dimensional stability of the polymeric materials in the presence of aggressive liquids.

The sorption behaviour in polymer blends was first reported by Cates and White.[11-13] They investigated the water sorption characteristics of polyacrylonitrile (PAN)/cellulose, PAN/silk and PAN/cellulose acetate blends. The sorption of water in PAN/cellulose and PAN/cellulose acetate varied linearly with blend composition while the blend of PAN/silk exhibited a complicated sorption behaviour. Hopfenberg *et al.*[14-17] systematically examined the effects of temperature, penetrant activity, blend composition and thermal history on the sorption kinetics of n-hexane in polystyrene/poly(2,6-dimethyl 1,4-phenylene oxide). The effect of fillers on the sorption behaviour of elastomers is also reported extensively.[18-20] It is observed that the presence of an active filler reduces the extent of equilibrium swelling compared to that of the corresponding gum sample.

Masuhara *et al.*[21] developed a membrane from poly(vinyl pyrrolidone) and polyurethane blend suitable for dialysis. The dialysis rate was found to be

approximately twice as high as rates normally achieved with conventional cellophane dialysis membranes. Hollow fibre dialysis membranes from a complicated blend of quaternised acrylonitrile-methyl vinyl pyridine copolymer and an acrylonitrile-vinyl acetate copolymer was reported by Sayler *et al.*[22] Molecular transport of alkanes[23] and haloalkanes[24] through blends of ethylene-propylene random copolymer and isotactic polypropylene has been reported by Aminabhavi *et al.* The sorption, desorption, resorption, and redesorption characteristics were influenced by the nature of the liquid and the temperature.

In this chapter, the diffusion and sorption behaviour of organic solvents through crosslinked nitrile rubber/poly(ethylene-co-vinyl acetate) (NBR/EVA) blends are dealt with. The effects of blend composition, crosslinking systems, filler type, filler loading, temperature and nature of penetrants on the diffusion process have been investigated.

7.1 Results and discussion

7.1.1 Sorption behaviour

The sorption behaviour of NBR/EVA blends in cyclohexanone as a function of blend composition, crosslinking systems, filler type and filler loading is studied. The effect of blend composition on the sorption behaviour of peroxide crosslinked system is presented in Figure 7.1. From Figure 7.1, it is observed that EVA has the lowest equilibrium uptake. There is an increase in the equilibrium uptake with the increase in NBR content. This can be related to the morphology of the system. The scanning electron micrographs of NBR/EVA blends is given in Figure 3.2. The schematic model for the morphology of crosslinked NBR/EVA blends is given in Figure 4.1

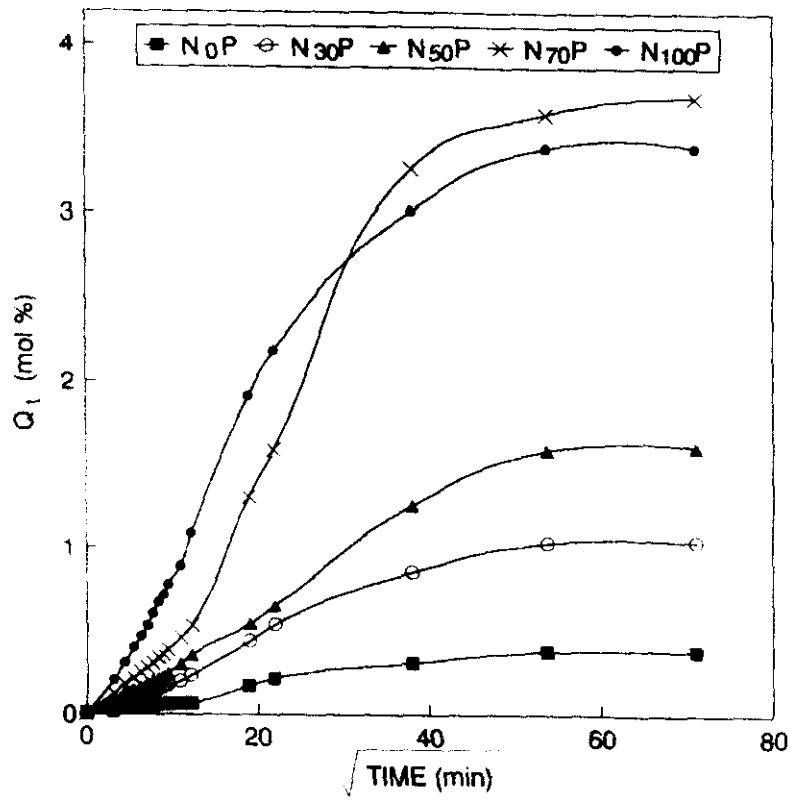

Figure 7.1. Sorption curves of NBR/EVA blends

The sorption behaviour of $N_{70}P$, where NBR is the continuous phase, is similar to that of NBR ($N_{100}P$). Again, the sorption behaviour of EVA rich blend ($N_{30}P$) is similar to that of EVA (N_0P). The $N_{50}P$, where both the phases are continuous, exhibits an intermediate sorption behaviour between those of the pure components. This clearly indicates that one can study the phase continuity from transport studies. But $N_{70}P$ (i.e. 70/30: NBR/EVA) exhibits a higher equilibrium uptake than $N_{100}P$ This can be explained on the basis of crosslink density. The crosslink density of the samples is calculated from the tensile measurements as explained in Section 2.3.7(a). The crosslink density values are given in Table 7.1. The higher equilibrium uptake of $N_{70}P$ is due to its lower crosslink density than $N_{100}P$. The equilibrium uptake is also affected by the crystallinity of the sample. EVA (N_0P) which is crystalline shows the lowest equilibrium uptake. As NBR is

added to EVA, the crystallinity is reduced and the equilibrium uptake increases accordingly

Table 7.1. Crosslink density (ν) and volume fraction of rubber (ϕ) in swollen mass of NBR/EVA blends.

Samples	ϕ	ν x 10^4 (gmol/cc)
N_0P	0.72	3.69
$N_{30}P$	0.48	3.02
$N_{50}P$	0.38	2.18
$N_{70}P$	0.19	1.44
$N_{100}P$	0.22	1.68
$N_{50}S$	0.39	2.27
$N_{50}M$	0.40	2.31
10S	0.44	5.54
10C	0.44	5.23
10BS	0.45	5.59
10BH	0.46	6.44
20BH	0.48	7.52
30BH	0.49	8.57

Volume fraction of rubber, ϕ, in the solvent swollen sample was calculated using the equation:[25]

$$\phi = \frac{w_1 / \rho_1}{w_1 / \rho_1 + w_2 / \rho_2} \qquad (7.1)$$

where w_1 is the weight of the rubber sample; ρ_1, density of the rubber; w_2, weight of solvent in the swollen sample and ρ_2, density of the solvent. A high value of ϕ is an indication of high crosslink density. The ϕ values are given in Table 7.1. The ϕ value also supports the higher equilibrium uptake of $N_{70}P$.

In spite of its higher equilibrium uptake value, $N_{70}P$ shows a lower initial rate of uptake than that of $N_{100}P$. This is due to the difference in solubility parameters (δ) of the samples, i.e., δ (cyclohexanone) - δ ($N_{70}P$) = 0.36 and δ(cyclohexanone) - $\delta(N_{100}P)$ = 0.12. The greater the difference in solubility parameter, the lesser the solubility of the solvent in the polymer. The difference in solubility parameters of the solvent and the polymer (δ_s–δ_p) is plotted against the equilibrium uptake and is given in Figure 7.2. It is clear from the figure that as δ_s–δ_p increases equilibrium uptake decreases. The higher equilibrium uptake of $N_{70}P$ is discussed earlier. The equilibrium uptake values of different NBR/EVA blends at various temperatures are given in Table 7.2. As expected, the equilibrium values increase with temperature.

Figure 7.3 shows the sorption curves of N_{50} with different crosslinking systems. Here the mixed cure system shows the lowest equilibrium uptake and peroxide cure system the highest. Sulphur cure system takes the intermediate position. The lowest equilibrium uptake of the mixed cure system is due to its high crosslink density (Table 7.1). The sorption curves of unfilled and various filled systems (10 phr loading) are given in Figure 7.4. The presence of fillers reduced the equilibrium uptake values considerably due to reinforcement. Among the various fillers, the HAF black filled system (10 BH) with the highest crosslink density shows the lowest equilibrium uptake. The equilibrium uptake of all the other filled systems (SRF black, silica and clay) are comparable. The extent of reinforcement was assessed using Kraus equation[20] as explained in Section 4.1.6(a) and it was found that as far as the extent of reinforcement is concerned, HAF is superior to other fillers. Thus the lower uptake of HAF filled system is supported by its reinforcing ability.

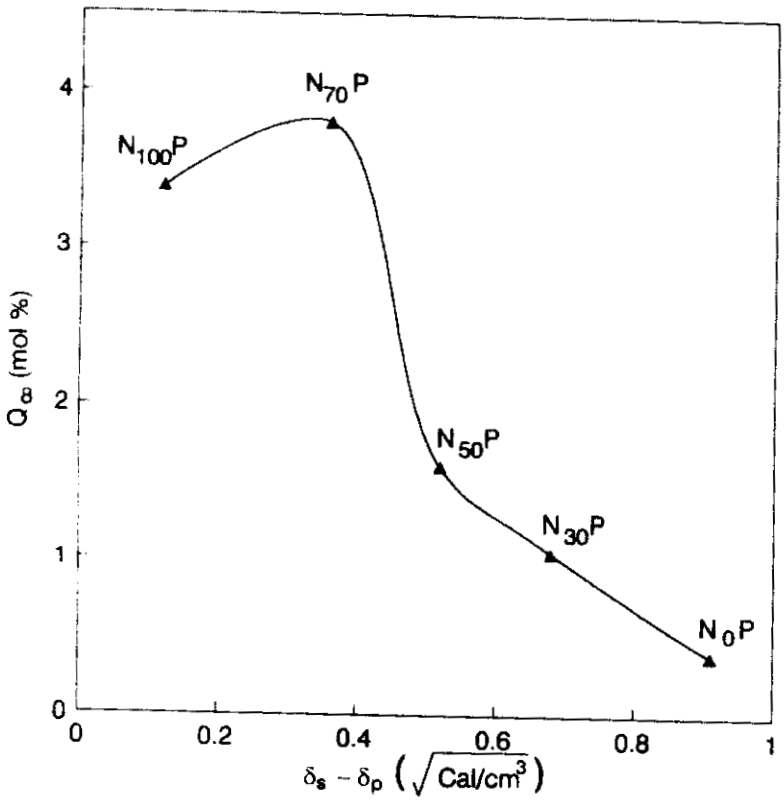

Figure 7.2. δ_s–δ_p vs. equilibrium uptake curve of NBR/EVA-cyclohexanone system

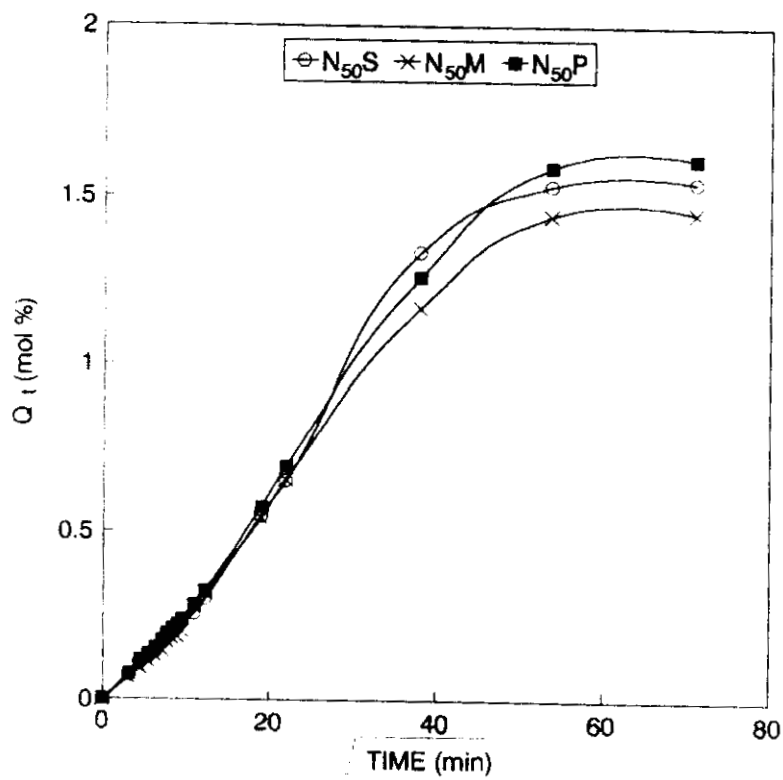

Figure 7.3. Sorption curves of various crosslinked NBR/EVA blends

Table 7.2. Dependence of equilibrium uptake (Q_∞) on temperature for NBR/EVA blends

Samples	27°C	40°C	50°C	60°C
N_0P	0.39	0.69	1.59	2.33
$N_{30}P$	1.05	1.56	3.16	5.39
$N_{50}P$	1.61	2.03	4.09	5.32
$N_{70}P$	3.81	3.89	5.60	7.52
$N_{100}P$	3.39	3.40	4.28	5.05
$N_{50}S$	1.54	1.82	2.84	4.23
$N_{50}M$	1.46	1.84	2.80	3.82
10S	1.14	1.42	1.99	3.12
10C	1.19	1.50	2.28	3.59
10BS	1.17	1.42	2.16	3.02
10BH	1.12	1.45	2.18	3.45
20BH	1.01	1.24	1.92	2.60
30BH	0.92	1.11	1.77	2.03

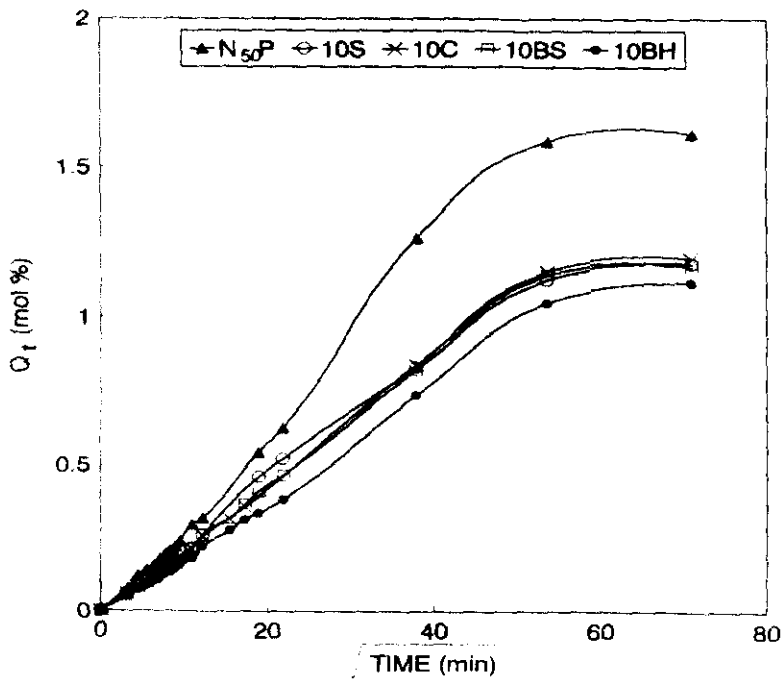

Figure 7.4. Sorption curves of unfilled and various filled NBR/EVA blends

With filler loading, there is a decrease in equilibrium uptake value (Figure 7.5). This is due to the increase in reinforcement with concentration.

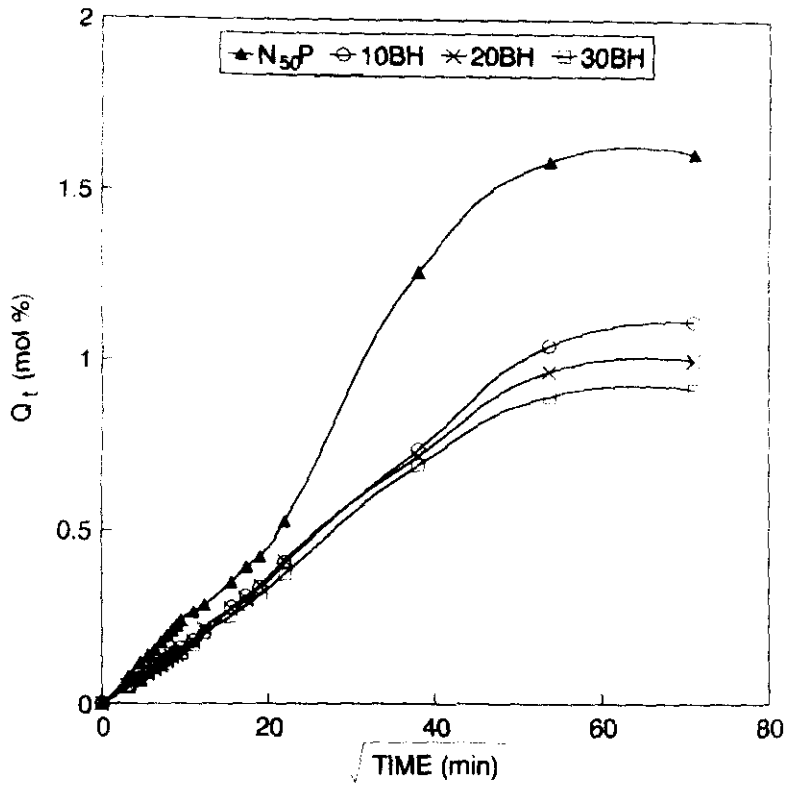

Figure 7.5. Effect of filler loading on the sorption curves

A schematic representation of the unfilled and filled blend before and after swelling is given in Figure 7.6. During mixing, carbon black forms bound rubber in the blend. Bound rubber represents the amount of polymer insolubilised by the carbon black. The decrease in equilibrium uptake of the filled system is due to the formation of bound rubber. As the reinforcement increases the bound rubber content also increases. The effect of temperature on the sorption curves of $N_{50}P$ is shown in Figure 7.7. The rate of diffusion and equilibrium uptake increase with increase in temperature. This behaviour is attributed to the increase in free volume and segmental mobility at higher temperature.

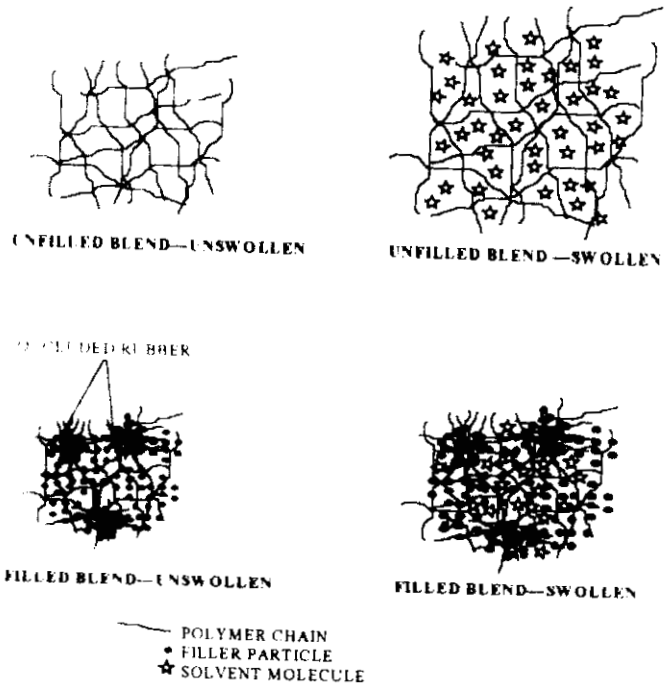

Figure 7.6. Schematic representation of unfilled and filled blends before and after swelling

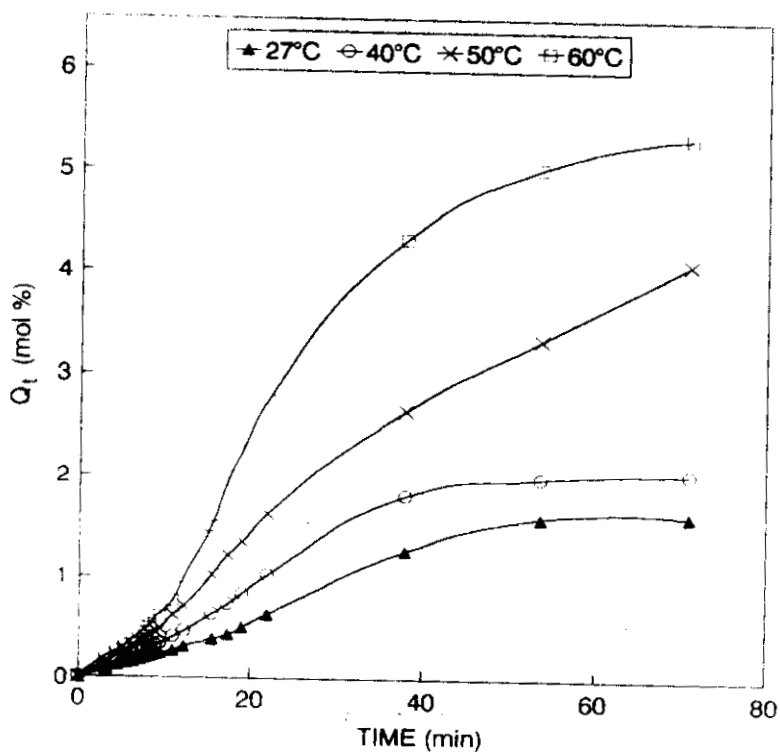

Figure 7.7. Effect of temperature on the sorption curves

To follow the mechanism of sorption, the values obtained are, fitted to the equation [26]

$$\log (Q_t/Q_\infty) = \log k + n \log t \qquad (7.2)$$

where Q_t is the mole per cent increase in uptake at time t; Q_∞, the mole per cent increase in uptake at equilibrium; t, the time; k, a constant characteristic of the polymer which indicates the interaction between polymer and solvent and n is a constant which indicates the mechanism of sorption. The values of n and k are determined by linear regression analysis and are given in Table 7.3.

Table 7.3. Values of n and k for NBR/EVA blends

Samples	n				k x 10^2 (min^{-n})			
	27°C	40°C	50°C	60°C	27°C	40°C	50°C	60°C
N_0P	0.45	0.50	0.58	0.56	1.8	2.0	1.3	1.5
$N_{30}P$	0.43	0.54	0.57	0.65	2.1	1.6	1.0	0.6
$N_{50}P$	0.42	0.55	0.61	0.62	2.0	1.4	0.8	0.7
$N_{70}P$	0.45	0.54	0.63	0.60	1.2	1.3	0.9	0.9
$N_{100}P$	0.51	0.62	0.65	0.59	2.0	1.5	1.3	1.5
$N_{50}S$	0.44	0.56	0.62	0.62	1.9	1.4	1.2	1.2
$N_{50}M$	0.43	0.57	0.64	0.52	1.8	1.5	0.9	1.6
10S	0.53	0.53	0.56	0.65	1.5	1.6	1.5	0.8
10C	0.52	0.57	0.54	0.64	1.4	1.4	1.6	0.8
10BS	0.55	0.56	0.55	0.60	1.3	1.3	1.6	1.0
10BH	0.54	0.55	0.49	0.62	1.2	1.4	1.8	1.1
20BH	0.53	0.56	0.52	0.58	1.4	1.3	1.7	1.2
30BH	0.57	0.57	0.50	0.56	1.4	1.4	1.9	1.5

For a Fickian diffusion mechanism, n has a value of 0.5. When n=1, the mechanism is non-Fickian and when it lies between 0.5 and 1, the diffusion is anomalous. From the table, it is observed that the values of n range from 0.42 to 0.65. For all the systems the n value is close to 0.5 at room temperature. This suggests the mode of diffusion is close to Fickian for cyclohexanone - NBR/EVA blend systems. However, a deviation from the Fickian mode of diffusion is observed as the temperature increases. No systematic trend is observed for the values of k at room temperature as well as at higher temperatures.

From the swelling data the diffusion coefficient, D is calculated using:[27]

$$D = \pi(h\theta/4Q_\infty)^2 \qquad (7.3)$$

where θ is the slope of the sorption curves before attainment of 50% equilibrium and h is the initial thickness of the sample. The value of D depends on the polymer segmental mobility. Equation (7.3) holds for systems without appreciable swelling. For considerable swelling, a correction for the swelling of the polymer can be made by incorporating ϕ, the volume fraction of the polymer in the swollen mass, thus giving the intrinsic diffusion coefficient, D*.[28]

$$D^* = \frac{D}{\phi^{7/3}} \qquad (7.4)$$

The values of intrinsic diffusion coefficients are given in Table 7.4. It is observed that the D* value increases with increase in NBR content in the blend. For the different crosslinking systems, the peroxide cured system ($N_{50}P$) exhibits the highest D* value. Among the filled systems, the silica filled system (1OS) shows a low D* value as the filler loading increases. For all the systems, D* value increases with increase in temperature which indicates the activation of diffusion process at higher temperatures.

The permeability of a penetrant in a polymer membrane depends on the diffusivity as well as solubility or sorption of the penetrant in the polymer membrane. Therefore, the sorption coefficient which is related to the equilibrium sorption of the penetrant is calculated using the equation,[29]

$$S = \frac{M_\infty}{M_p} \tag{7.5}$$

where M_∞ is the mass of the solvent taken up at equilibrium swelling and M_p is the mass of the polymer sample. The permeability coefficient (P) which implies the net effect of sorption and diffusion is given by the relation.[25]

$$P = D^*S \tag{7.6}$$

The values of S and P are given in Table 7.4. A similar trend as that of D* is observed for S and P values with the change in blend composition, crosslinking systems, filler type, filler loading and temperature. The variation in sorption coefficient (S) with the weight percentage of NBR is given in Figure 7.8. The value of S increases with NBR content. The effect of weight percentage of NBR on intrinsic diffusion (D*) and permeation (P) coefficients is shown in Figure 7.9. D* and P increase regularly up to 50 wt% of NBR. Beyond that the properties increase sharply. This can be attributed to the phase inversion in morphology of the system.

Table 7.4. Values of intrinsic diffusion, sorption and permeation coefficients for NBR/EVA blends

Samples	D* x 10^7 ($cm^2 s^{-1}$)				S				P x 10^6 ($cm^2 s^{-1}$)			
	Temperature (°C)											
	27	*40*	*50*	*60*	*27*	*40*	*50*	*60*	*27*	*40*	*50*	*60*
N_0P	0.63	4.04	18.64	24.06	0.38	0.67	1.56	2.29	0.02	0.27	2.91	5.51
$N_{30}P$	1.43	9.04	24.50	66.44	1.03	1.53	3.09	5.28	0.15	1.38	7.57	35.08
$N_{50}P$	2.11	13.23	42.18	67.15	1.58	1.98	4.00	5.22	0.33	4.62	16.87	35.06
$N_{70}P$	5.52	34.11	124.82	174.79	3.75	3.81	5.48	7.36	2.07	12.99	68.40	128.64
$N_{100}P$	17.27	63.69	121.62	118.94	3.32	3.31	4.20	4.94	5.73	21.08	51.08	58.75
$N_{50}S$	2.04	12.44	45.47	97.88	1.51	1.78	2.78	4.14	0.31	3.02	12.64	40.52
$N_{50}M$	1.95	14.85	39.11	52.89	1.42	1.87	2.85	3.74	0.28	2.77	11.15	19.78
10S	4.79	9.94	24.79	48.67	1.11	1.38	1.94	3.06	0.53	1.37	4.81	14.52
10C	4.86	9.66	21.91	41.38	1.17	1.47	2.23	3.51	0.57	1.42	4.89	14.52
10BS	4.93	9.72	23.83	41.29	1.14	1.39	2.12	2.95	0.56	1.28	5.05	12.18
10BH	4.91	9.96	19.32	62.35	1.09	1.42	2.13	3.38	0.53	1.41	4.11	21.07
20BH	4.49	9.53	18.80	37.11	0.98	1.21	1.87	2.55	0.44	1.15	3.52	9.46
30BH	4.77	9.40	15.87	30.17	0.90	1.09	1.73	1.99	0.43	1.02	2.69	6.00

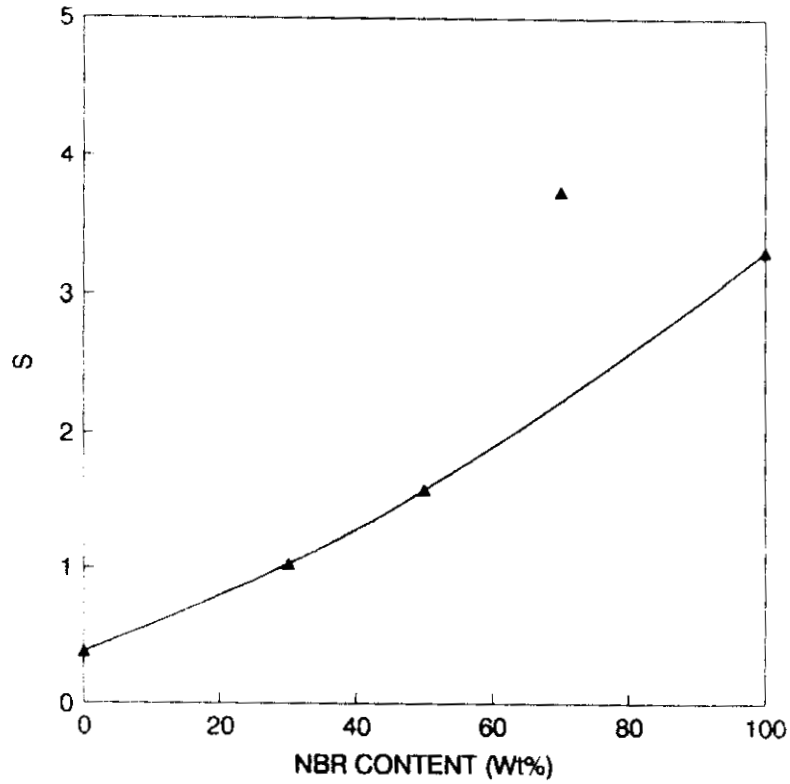

Figure 7.8. Variation of S with the weight percentage of NBR

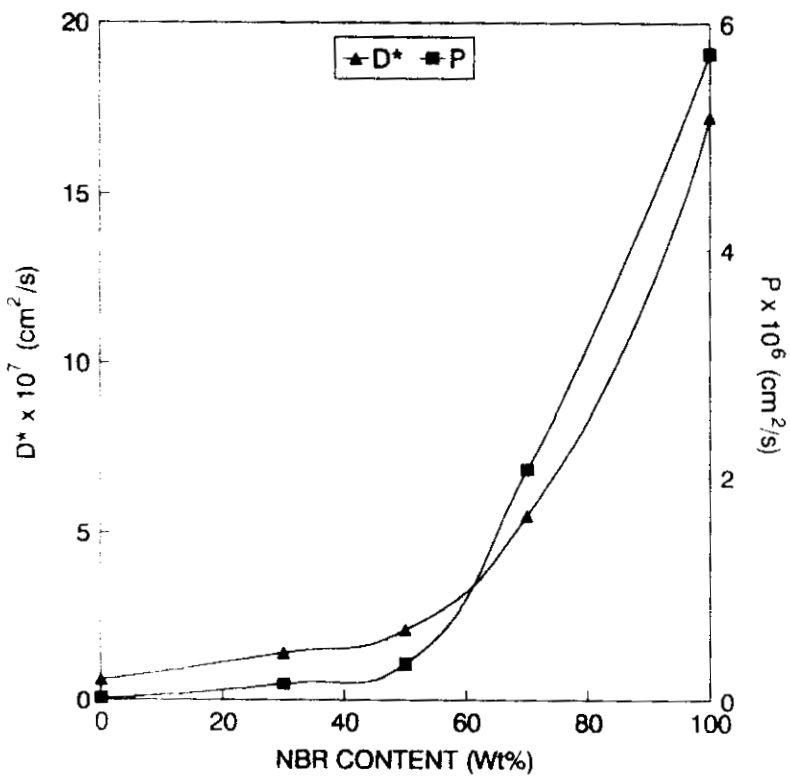

Figure 7.9. Variation of D* and P with the weight percentage of NBR

In the case of heterogeneous blends, the permeability can be interpreted in terms of various theoretical models. The Robeson's two limiting models, i.e., series and parallel models are generally used in the case of polymer blends.[30]

According to parallel model

$$P_c = P_1\phi_1 + P_2\phi_2 \tag{7.7}$$

and by series model

$$P_c = P_1P_2 / (\phi_1P_2/\phi_2P_1) \tag{7.8}$$

where P_c, P_1 and P_2 are the permeation coefficients of blend, component I and component II respectively and ϕ_1 and ϕ_2 are the volume fractions of components I and II respectively.

Further, for a conducting spherical filler, the overall composite permeation coefficient is given by Maxwell's equations as[30,31]

$$\bar{P}_c = P_m \frac{P_d + 2P_m - 2\phi_d(P_m - P_d)}{P_d + 2P_m + \phi_d(P_m - P_d)} \tag{7.9}$$

where the subscripts d and m correspond to dispersed phase and matrix respectively

Robeson extended[31] Maxwell's analysis to include the continuous and discontinuous characteristic of both phases at intermediate compositions and expressed the equation,

$$\bar{P}_c = \chi_a\bar{P}_1\left[\frac{\bar{P}_2 + 2\bar{P}_1 - 2\phi_2(\bar{P}_1 - \bar{P}_2)}{\bar{P}_2 + 2\bar{P}_1 + \phi_2(\bar{P}_1 - \bar{P}_2)}\right] + \chi_b\bar{P}_2\left[\frac{\bar{P}_1 + 2\bar{P}_2 - 2\phi_1(\bar{P}_2 - \bar{P}_1)}{\bar{P}_1 + 2\bar{P}_{21} + \phi_1(\bar{P}_2 - \bar{P}_1)}\right] \tag{7.10}$$

where χ_a and χ_b are fractional contributions to continuous phase so that $\chi_a + \chi_b = 1$.

Figure 7.10 shows the variation of permeation coefficient with volume fraction of NBR. The experimental values are close to the Maxwell model up to $\phi_{NBR} = 0.6$ and beyond that it is close to Robeson model.

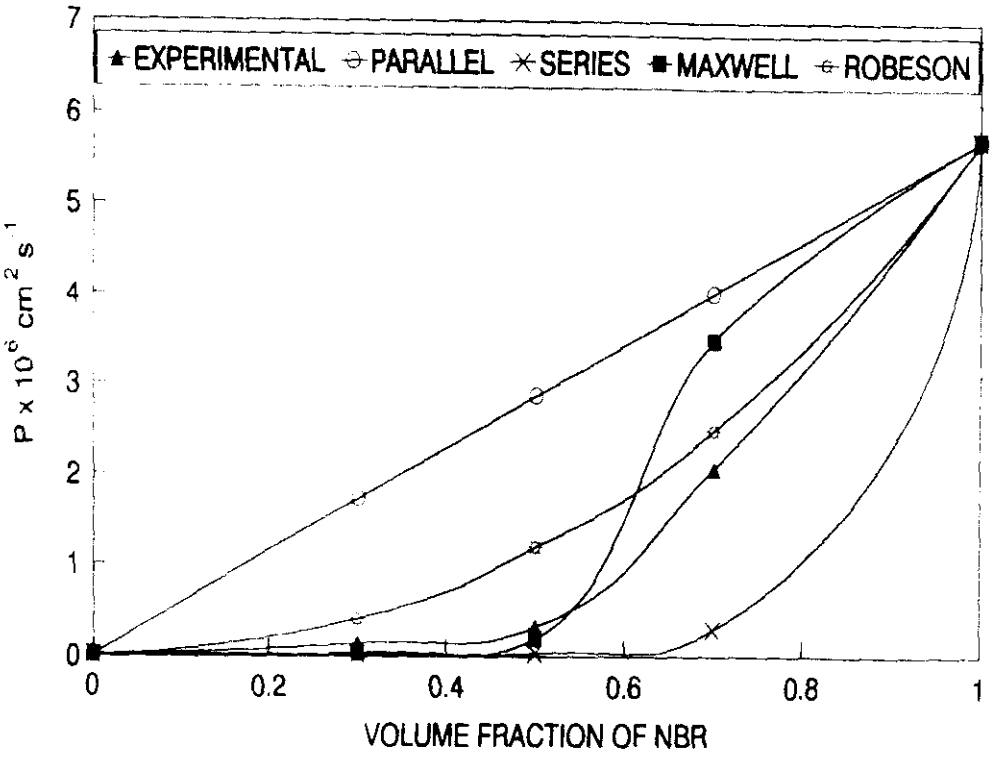

Figure 7.10. Theoretical modelling for the permeation coefficient of NBR/EVA blends

The temperature dependence of transport coefficients (D*, S and P) can be used to calculate the energy of activation for the processes of diffusion and permeation from the Arrhenius relationship given in Section 6.1.2. Here X is D*, S or P. The values of activation energy of permeation (E_P) and the activation energy of diffusion (E_D) are given in Table 7.5. Pure EVA (N_0P) exhibits the highest activation energy for both permeation and diffusion. This is because of the crystalline nature of EVA. E_P and E_D decrease as the weight per cent of NBR increases. As the NBR content is increased, the crystallinity of the sample is reduced and hence the blends exhibit drop in activation energies. This is evident

from the X-ray diffraction patterns given in Figure 7.11. The X-ray diffraction patterns are separated into two parts, crystalline and amorphous, by taking nitrile rubber as fully amorphous. The area under the crystalline and amorphous portions is measured in arbitrary units, and the degree of crystallinity X_c of the samples is calculated using the relation:

$$X_c = \frac{I_c}{I_c + I_a} \tag{7.11}$$

where I_c and I_a represent the integrated intensities corresponding to the crystalline and amorphous phases respectively, i.e., the area under the respective curves. The degree of crystallinity (X_c), of N_0P, $N_{30}P$, $N_{50}P$ and $N_{70}P$ is 35, 23, 20 and 8%, respectively.

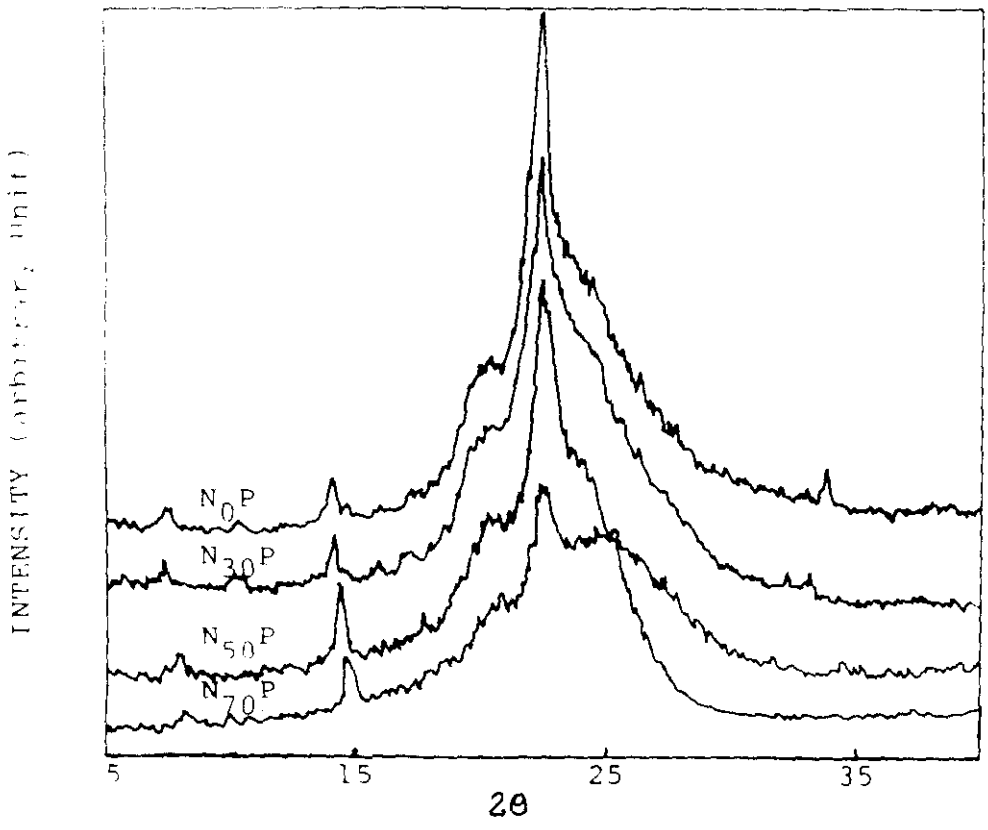

Figure 7.11. XRD patterns of NBR/EVA blends

Table 7.5. Activation energies for permeation and diffusion of NBR/EVA blends

Samples	E_P (kJ mol^{-1})	E_D (kJ mol^{-1})
N_0P	96.9	144.2
$N_{30}P$	95.9	139.4
$N_{50}P$	90.7	122.1
$N_{70}P$	90.8	108.5
$N_{100}P$	50.9	61.5
$N_{50}S$	99.8	124.3
$N_{50}M$	85.5	110.7
10S	59.9	85.4
10C	55.2	83.1
10BS	56.4	80.3
10BH	62.8	91.5
20BH	53.6	78.6
30BH	46.2	67.7

Usually the activation energies for permeation and diffusion increase with loading. But in the case of $N_{50}P$ as the carbon black loading is increased from 10 BH to 30 BH, it is seen that there is a decrease in E_P and E_D. This is due to the presence of polar groups on the surface of carbon black which enables a high interaction with cyclohexanone, a polar solvent. As the loading is increased the number of filler particles per unit volume increases, thereby increasing the sites of interaction. However, the equilibrium uptake exhibits the normal trend, i.e. decreases with filler loading as observed earlier.

The enthalpy and entropy of sorption have been calculated using the Van't Hoff relation[27]

$$\ln K_s = \frac{\Delta S}{R} - \frac{\Delta H}{RT} \qquad (7.12)$$

The values obtained by linear regression method are given in Table 7.6. It is found that the values of ΔH and ΔS are positive for the different NBR/EVA systems

Table 7.6. Thermodynamic parameters

Samples	ΔH (kJ mol^{-1})	ΔS ($Jmol^{-1}$ k^{-1})
N_0P	47.2	110.6
$N_{30}P$	42.4	102.4
$N_{50}P$	32.2	72.3
$N_{70}P$	17.8	45.6
$N_{100}P$	10.5	6.5
$N_{50}S$	26.1	51.1
$N_{50}M$	25.1	47.9
10S	25.3	46.2
10C	25.1	55.8
10BS	24.5	44.1
10BH	28.5	56.8
20BH	24.7	43.3
30BH	21.5	32.1

7.1.2 Determination of the network structure

The investigation of swelling equilibrium can help to elucidate the structure of the polymer network. Flory and Rehner[32] relations were developed for a network deforming affinely, i.e., the components of each chain vector transform linearly with macroscopic deformation and the junction points are assumed to be embedded in the network without fluctuations. Then the molecular weight between crosslinks (M_c) for the affine limit of the model [M_c(aff)] is calculated by the formula.[33]

$$M_c\,(\text{aff}) = \frac{\rho V_s \nu_{2c}^{2/3} \nu_{2m}^{1/3}\left(1 - \frac{\mu}{\nu}\nu_{2m}^{1/3}\right)}{-\left(\ln(1-\nu_{2m}) + \nu_{2m} + \chi\nu_{2m}^2\right)} \tag{7.13}$$

where V_s is the molar volume of the solvent, μ and ν are called the number of effective chains and junctions; ν_{2m}, the polymer volume fraction at swelling equilibrium, ν_{2c}, the polymer volume fraction during crosslinking; and ρ, the polymer density. James and Guth[34] proposed the phantom network model, where the chain may move freely through one another. According to the theory, the molecular weight between crosslinks for the phantom limit of the model [M_c(ph)] is calculated by[33]

$$M_c\,(\text{ph}) = \frac{\left(1 - \frac{2}{\phi}\right)\rho V_s \nu_{2c}^{2/3} \nu_{2m}^{1/3}}{-\left(\ln(1-\nu_{2m}) + \nu_{2m} + \chi\nu_{2m}^2\right)} \tag{7.14}$$

where ϕ is the junction functionality.

M_c(aff) and M_c(ph) are compared with M_c(chem) and the values are given in Table 7.7. It is seen that M_c(chem) values are close to M_c(aff). This suggests that in the highly swollen state, the chains in NBR, EVA and the blends deform affinely.

Table 7.7. Comparison of network structure

Sample	M_c(chem.)	M_c(affine)	M_c(phantom)
N_0P	296	288	96
$N_{30}P$	960	935	311
$N_{50}P$	1761	1715	572
$N_{70}P$	8324	8101	2700
$N_{100}P$	5295	5153	1717
$N_{50}S$	1658	1557	579
$N_{50}M$	1536	1411	470
10S	1214	1116	371
10C	1243	1142	381
10BS	1169	1073	358
10BH	1098	1008	336
20BH	998	867	289
30BH	985	813	271

7.1.3 Comparison with theory

The experimental diffusion results are compared with theoretical predictions in order to find the deviation from the regular Fickian mode described by the equation[35]

$$\frac{M_t}{M_\infty} = 1 - \frac{8}{\pi^2}\sum_{n=0}^{n=\infty}\frac{1}{(2n+1)^2}\exp\left[\frac{-D(2n+1)^2\pi^2 t}{h^2}\right] \qquad (7.15)$$

The given equation represents a Fickian mode of diffusion. Figure 7.12 shows the experimental (at room temperature) and theoretical sorption curves. This is excellent fit at the early stages of diffusion indicating Fickian behaviour. However, at longer time some deviation could be observed.

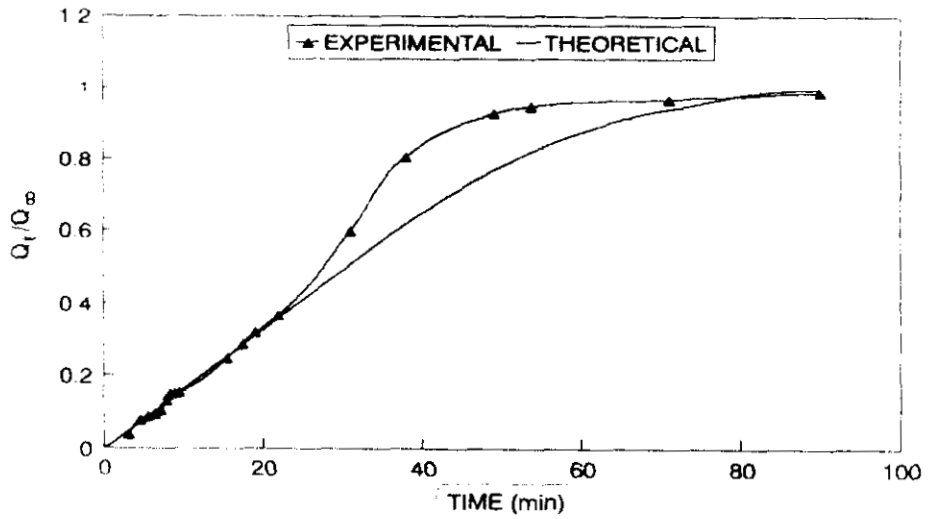

Figure 7.12. Comparison of theoretical and experimental sorption curves

7.1.4 Effect of penetrants

Dichloromethane, chloroform and carbon tetrachloride are used to study the effect of penetrants. The sorption curves as a function of blend composition are given in Figures 7.13–7.15.

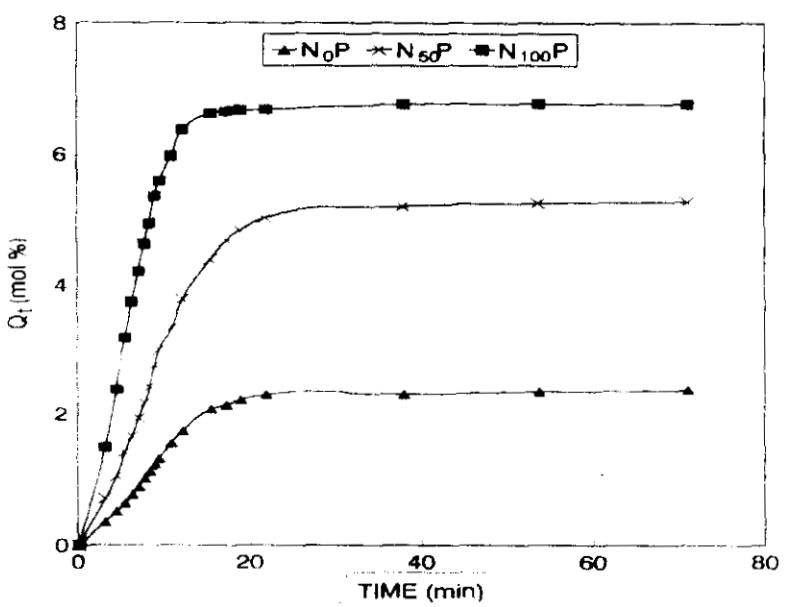

Figure 7.13. Sorption behaviour of NBR/EVA blends in dichloromethane

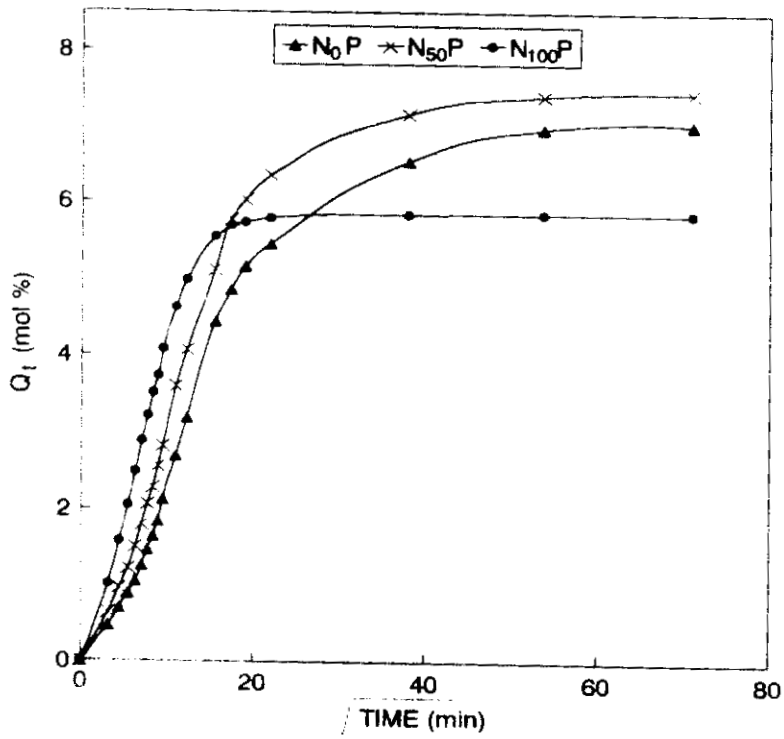

Figure 7.14. Sorption behaviour of NBR/EVA blends in chloroform

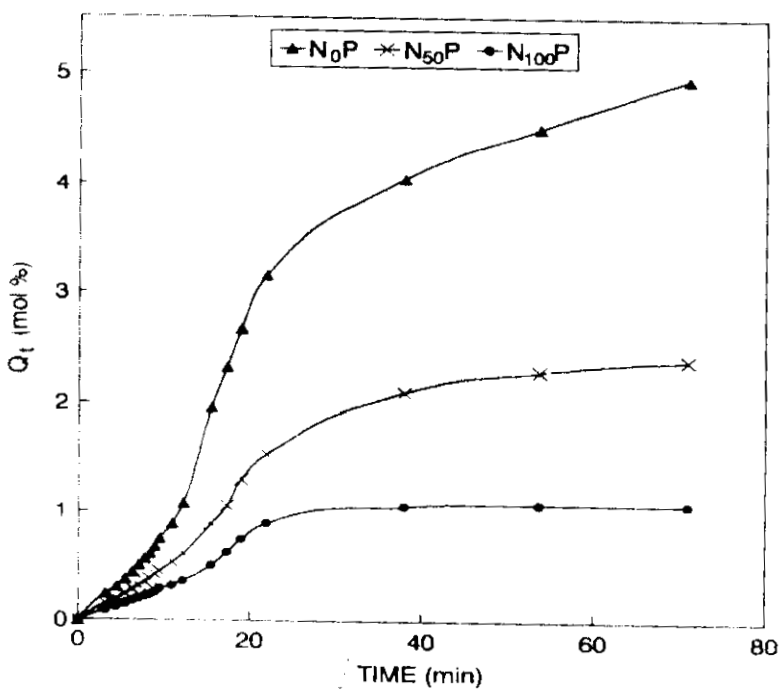

Figure 7.15. Sorption behaviour of NBR/EVA blends in carbon tetrachloride

In dichloromethane N_0P (Pure EVA) exhibits the lowest uptake (Figure 7.13). The rate of diffusion as well as the equilibrium uptake increase with the increase in NBR content. This can be explained on the basis of solubility parameters of the solvent and polymers. The closer the solubility parameters, greater will be the solubility of the solvent in the polymer. The solubility parameters of the solvents and polymers are given in Table 7.8. In the case of chloroform (Figure 7.14) the equilibrium uptake is higher for the blend than that of the pure components. This is because of the closeness in solubility parameters of $N_{50}P$ and chloroform. In carbon tetrachloride, the rate of diffusion as well as the equilibrium uptake increase with the increase in EVA content (Figure 7.15). The values of Q_∞ in different solvents are given in Table 7.9.

Table 7.8. Solubility parameters (δ) of solvents and polymers

Reference	δ (cal/cm^3)$^{1/2}$
Dichloromethane	9.7
Chloroform	9.3
Carbon tetrachloride	8.6
N_0 (pure EVA)	8.99
N_{50} (50/50 NBR/EVA)	9.38
N_{100} (pure NBR)	9.78

Table 7.9. Values of Q_∞ in different solvents

Samples	Dichloromethane	Chloroform	Carbon tetrachloride
N_0	2.38	7.03	4.95
N_{50}	5.28	7.45	2.41
N_{100}	6.77	5.87	1.08

The equilibrium uptake of the blends in dichloromethane, chloroform and carbon tetrachloride is plotted against the difference in solubility parameters of the

solvent and polymer in Figures 7.16–7.18, respectively. Greater the difference, lesser the equilibrium uptake.

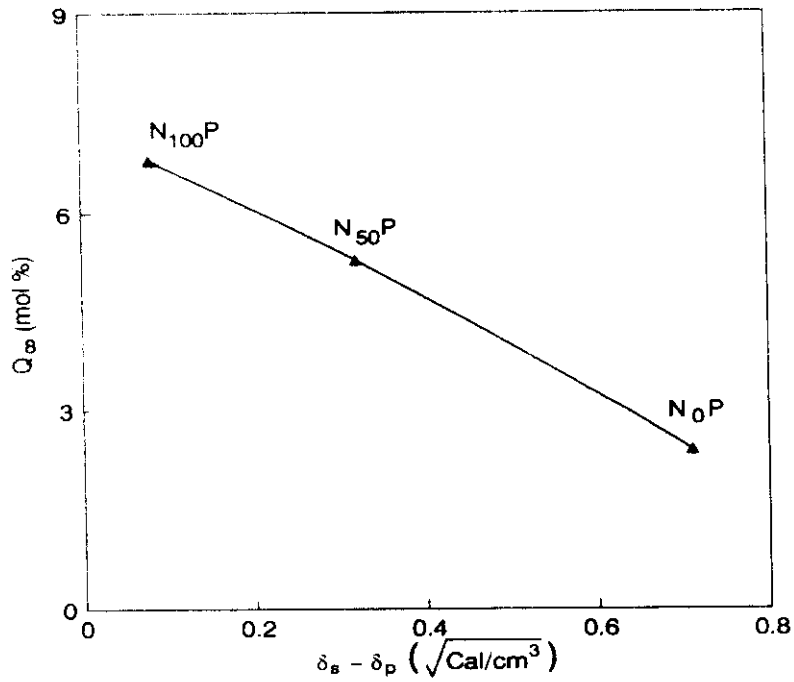

Figure 7.16. δ_s–δ_p vs. equilibrium uptake curve for NBR/EVA-dichloromethane system

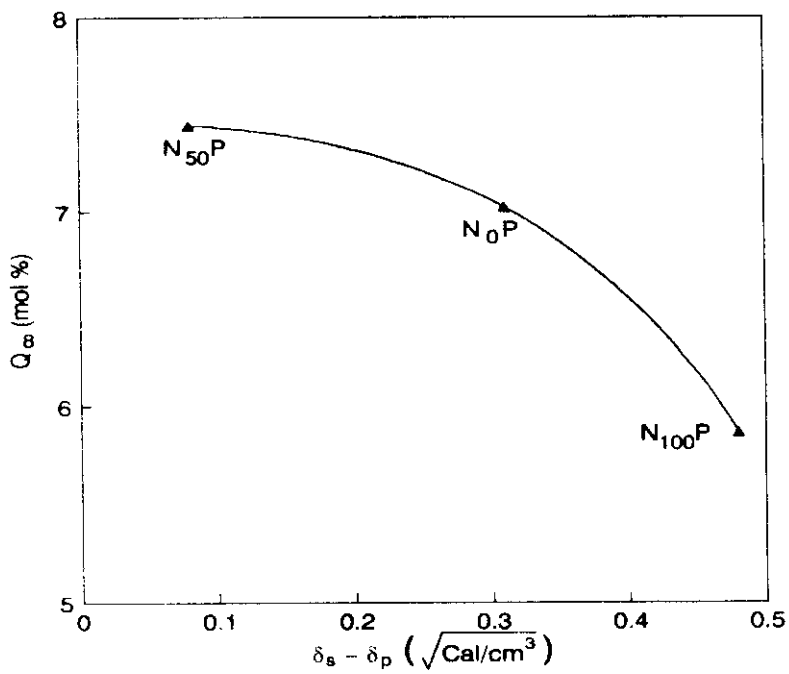

Figure 7.17. δ_s–δ_p vs. equilibrium uptake curve for NBR/EVA-chloroform system

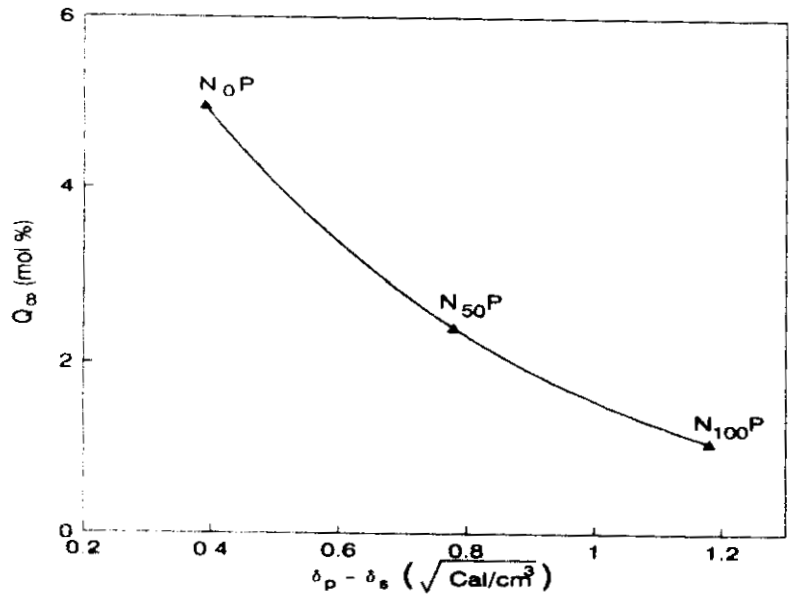

Figure 7.18. δ_p–δ_s vs. equilibrium uptake curve for NBR/EVA-carbon tetrachloride system

The sorption curves of $N_{50}P$ for different penetrants are shown in Figure 7.19. Here also solubility parameter is the deciding factor for the rate of diffusion and equilibrium uptake.

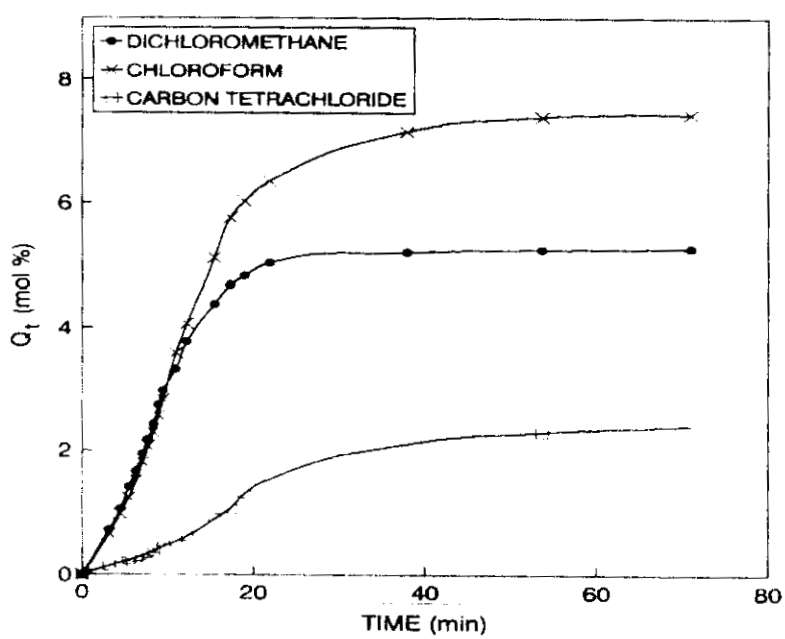

Figure 7.19. Sorption curves of $N_{50}P$ in different solvents

The mechanism of sorption is followed by fitting the values obtained in equation (7.2). The values of n and k are given in Table 7.10. The values of n lie between 0.5 and 1 for all the solvents indicating a deviation from the Fickian mode of diffusion.

Table 7.10. Values of n and k in different solvents

Samples		n	k x 10^2 (gg^{-1} min^{-1})
Dichloromethane	N_0	0.55	4.1
	N_{50}	0.62	3.1
	N_{100}	0.68	4.6
Chloroform	N_0	0.65	1.4
	N_{50}	0.66	1.8
	N_{100}	0.63	4.0
Carbon tetrachloride	N_0	0.64	0.9
	N_{50}	0.57	1.4
	N_{100}	0.54	2.1

In order to understand the stability of the membranes, the sorption-desorption-resorption-redesorption pattern of $N_{50}P$ in carbon tetrachloride is followed and is presented in Figure 7.20. The figure reveals that the rates for desorption and redesorption is greater than those for sorption and resorption. In the sorption process, the solvent molecules have to penetrate into the tightly packed network and hence the rate for the sorption process is low. While in the desorption process, the escape of solvent molecules from the relaxed polymer chain takes place more easily. So the rate of desorption processes are greater than those for sorption processes.

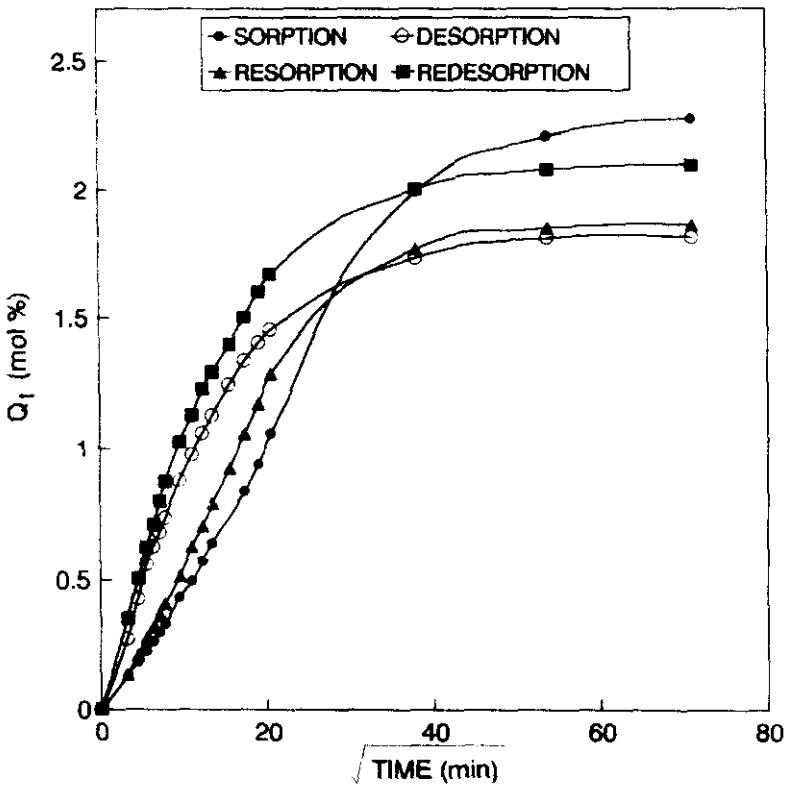

Figure 7.20. Sorption-desorption-resorption-redesorption curves of $N_{50}P$ in carbon tetrachloride

7.2 References

1. N. S. Schneider, J. L. Illinger and M. A. Cleaves, *Polym. Eng. Sci.*, **26**, 22 (1986).
2. L. A. Errede, *Macromolecules*, **19**, 654 (1986).
3. S. B. Harogoppad and T. M. Aminabhavi, *J. Appl. Polym. Sci.*, **42**, 2329 (1991).
4. A. R. Berens and H. B. Hopfenberg, *Polymer*, **19**, 489 (1978).
5. Yi-Yan, R. M. Fielder and W. J. Koros, *J. Appl. Polym. Sci.*, **25**, 1755 (1980).
6. M. O. David, Q. T. Nguyen and J. Neel, *J. Membr. Sci.*, **73**, 129 (1992).
7. J. Landois-Gavza and J. H. Hotchkiss, *Food and Packaging Interactions*, ACS, Symposium Series 365, Am. Chem. Soc., Washington, DC, 1987, p. 53.

8. P. V. Kulkarni, S. B. Rajar, P. Antich, T. M .Aminabhavi and M. I. Aralaguppi, *J. Macromol. Sci. Rev. Macromol. Chem. Phys. C*, **30**, 441 (1990).

9. H. Kawai, T. Soen, F. Fujimoto and T. Shiroguchi, *Japanese Patent* No. 100, 780 (1973); *Chem. Abstr.*, **80**, 10946g (1974).

10. H. Coll and C. G. Searles, *Polymer*, **29**, 1266 (1988).

11. D. M. Cates and H. J. Jr. White, *J. Polym. Sci.*, **20**, 181 (1956).

12. D. M. Cates and H. J. Jr. White, *J. Polym. Sci.*, **20**, 155 (1956).

13. D. M. Cates and H. J. Jr. White, *J. Polym. Sci.*, **21**, 125 (1956).

14. C. H. M. Jacques, H. B. Hopfenberg and V. Stannett, *Polym. Eng. Sci.*, **13**, 81 (1973).

15. C. H. M. Jacques and H. B. Hopfenberg, *Polym. Eng. Sci.*, **14**, 441 (1974).

16. C. H. M. Jacques and H. B. Hopfenberg, *Polym. Eng. Sci.*, **14**, 449 (1974).

17. H. B. Hopfenberg, V. T. Stannett and G. M. Folk, *Polym. Eng. Sci.*, **15**, 261 (1975).

18. R. F Fedors, *Polymer*, **20**, 126 (1979).

19. S. S. Sternstein, *J. Macromol. Sci. (B)*, **6**, 243 (1972).

20. G. Kraus, *J. Appl. Polym. Sci.*, 7, 861 (1963).

21. E. Masuhara, N. Nakaboyoshi, Y. Imai, A. Watanabe and S. Kazem, *Japanese Patent* No. 88, 077 (1973); *Chem. Abstr.*, **80**, 10946g (1974).

22. T. O. Sayler, J. S. Tapp and W. E. Weesner, *Us Patent* No. 3, 799, 356 (March 26, 1974), *Chem. Abstr.*, **81**, 26689d (1974).

23. T. M. Aminabhavi and H. T. S. Phayde, *J. Appl. Polym. Sci.*, **55**, 1335 (1995).

24. T. M. Aminabhavi and H. T. S. Phayde, *J. Appl. Polym. Sci.*, **57**, 1491 (1995).

25. P. E. Cassidy, T. M. Aminabhavi and C. M. Thompson, *Rubber Chem. Technol.* **56**, 594 (1983).

26. J. S. Chion and D. R. Paul, *Polym. Eng. Sci.*, **26**, 1218 (1986).

27. T. M. Aminabhavi and R. S. Khinnavar, *Polymer*, **34**, 1006 (1993).

28. W. R. Brown, R. B. Jenkins and G. S. Park, *J. Polym. Sci. -Symp.*, **41**, 45 (1973)

29. U. S. Aithal, T. M. Aminabhavi and P. E. Cassidy, *Am. Chem. Soc. Symp. Ser.*, **423**, 351 (1990).

30. H. B. Hopfenberg and D. R. Paul, in *Polymer Blends*, Vol. 1, (Ed., D. R. Paul), Academic Press, New York, 1976.

31. L. M. Robeson, A. Noshay, M. Matzner and C. N. Merriam, *Die. Angew. Makromol. Chem.*, **29/30**, 47 (1973).

32. P. J. Flory, *Principles of Polymer Chemistry*, Cornell University Press, Ithaca, 1953

33. L. R. G. Treloar, *The Physics of Rubber Elasticity*, Clarendon Press, Oxford, 1975

34. H. M. James and E. Guth, *J. Chem. Phys.*, **15**, 669 (1947).

35. U. S. Aithal, T. M. Aminabhavi and P. E. Cassidy, *J. Chem. Educ.*, **67**, 82 (1990).